SI Appendix for

Direct high-resolution mapping of electrocatalytic activity of semi-two-dimensional catalysts with single-edge sensitivity

Tong Sun[1,2,‖], Dengchao Wang[1,‖], Michael V. Mirkin[1,2]*, Hao Cheng[3], Jin-Cheng Zheng[3]*, Ryan M. Richards[4], Feng Lin[5], and Huolin L. Xin[6, 7]*

1. Department of Chemistry and Biochemistry, Queens College, CUNY, Queens, NY 11367

2. Ph.D. Program in Chemistry, The Graduate Center of the City University of New York, New York, NY 10016

3. Department of Physics, Xiamen University, Xiamen, China 361005

4. Department of Chemistry, Colorado School of Mines, Golden, CO 80804

5. Department of Chemistry, Virginia Tech, Blacksburg, VA 24061

6. Department of Physics and Astronomy, University of California, Irvine, CA 92697

7. Center for Functional Nanomaterials, Brookhaven National Laboratory, Upton, NY 11973

‖ These authors contributed equally.

This document contains:

Supplementary movie captions,
supplementary methods and supplementary figures
COMSOL simulation report

Supplementary Movie Captions:

Movie S1. 3D visualization of the NiO nanosheet structure. (The stray intensity cloud outside the nanosheet are artifacts resulted from the missing wedge.)

Movie S2. Close-up view of the nanosheet edge structures.

Movie S3. Close-up view of the nanosheet edge structures.

Movie S4. Close-up view of the nanosheet edge structures.

Movie S5. Close-up view of the nanosheet edge structures.

Movie S6. An atomistic view of the edge termination.

Supplementary methods:

Synthesis. NiO nanosheets were prepared using a two-step method. An alcohol pseudosupercritical drying technique was used to synthesize nickel hydroxide from $Ni(NO_3)_2$. Briefly, $Ni(NO_3)_2 \cdot 6H_2O$, urea and benzyl alcohol was added into 50 ml of methanol with a molar ratio of 2:1:4 in an autoclave (Parr Reactor). The reactor was then filled with 9 bars of Ar. Then, the mixture was heated to 265 ^{o}C and maintained at the temperature for 1.5 hours. Finally, the vapor inside was vented (i.e., pseudosupercritical drying). A green powder (nickel hydroxide) was collected and subsequently calcined at 500 ^{o}C for 6 hours to yield NiO nanosheets.

Materials. Ferrocenemethanol (Fc, 99%, Sigma-Aldrich) was sublimed before use. KOH (99%), KCl (99%), methanol (>99.8%) purchased from Sigma-Aldrich were used as received. Highly oriented pyrolytic graphite (HOPG) obtained from K-Tek was of ZYB grade.

Electrodes and electrochemical experiments. Polished Pt disk electrodes were fabricated by pulling 12.5-μm-radius annealed Pt wires into borosilicate glass capillaries (0.3 mm I.D. and 1.0 mm O.D.) with a P-2000 laser pipette puller (Sutter Instrument Co.) and polishing under video microscopic control as described previously. In this way, the electrodes can be prepared with radii

varying from 3 nm to 200 nm and RG (i.e. the ratio of the insulator radius to that of the Pt disk) from 6 to 15.[1] The voltammograms were obtained with a BAS-100B electrochemical workstation (Bioanalytical Systems, West Lafayette, IN) inside a Faraday cage. A 0.25 mm diameter Ag wire coated with AgCl served as a reference electrode.

Substrate preparation. NiO nanosheets were first dispersed in methanol under sonication and then drop cast on the HOPG surface. When the entire surface of the mm-sized HOPG substrate was covered with NiO sheets, the very large water oxidation current resulted in high concentration of oxygen in solution and high background current at the tip electrode. To avoid this problem, a micrometer-sized spot covered by NiO sheets was created by touching the HOPG surface with the tip of a micrometer-sized glass pipette containing dispersed NiO sheets. This process was controlled using a long-distance video microscope.

SECM setup and procedures. SECM experiments were carried out using a home-built instrument, which was similar to that described previously.[2] The nanoelectrode used as an SECM tip was positioned a few tens of micrometres above the substrate surface. A long-distance video microscope was used to monitor the initial approach of the SECM tip to the substrate. The tip was then brought closer to the substrate in an automated mode until the monitored tip current changed by 10%. The current-distance curves and constant-height SECM images were obtained during the subsequent fine approach. All experiments were carried out at room temperature (23 ± 2 °C) inside a Faraday cage. To prevent possible damage to the glass-sealed nanoelectrodes, the KOH concentration in OER experiments was 1 mM.

TEM and AFM Imaging. An XE-120 scanning probe microscope (Park Systems) was employed for imaging the nanoelectrodes and the HOPG substrate. PPP-NCHR AFM probes (Nanosensors) were used for noncontact imaging. The procedures for AFM imaging of nanoelectrodes were

reported previously.[3] The high-resolution annular dark-field scanning transmission electron microscopy (STEM) imaging of the NiO thin slabs were performed using a probe-corrected cold-field-emission dedicated STEM operated at 200 keV.

TEM tomography. TEM tomography tilt series acquisition was performed in FEI Talos F200X operated at 200 keV. Images were acquired from -70 degrees to +70 degrees with two-degree tilt intervals. The 3D tomograms were reconstructed by a home-written Matlab code implementing the multiplicative simultaneous iterative reconstruction technique (M-SIRT) and visualized by Avizo.[4]

Characterization of nanoelectrodes. The nanoelectrode tips were characterized by voltammetry and AFM imaging. An AFM image of the ~80-nm-radius polished Pt electrode employed in NiO/HOPG imaging (Fig. 2 in the main text) is shown in Figure S4a. From the cross-section in Fig. S4a one can see that this electrode was essentially flat (the recess depth ~4 nm) and well-polished. The effective tip radius calculated from the plateau current of the steady-state voltammogram in panel B (~ 80 nm) is in good agreement with the AFM image. Smaller (e.g. 20 nm radius) nanoelectrodes were characterized similarly (Figure S10).

SECM feedback responses at NiO and HOPG with the ferrocenemethanol mediator. As shown in Fig. S2, the SECM feedback was positive feedback when the tip approached the conductive HOPG surface (black curve) and negative over the semiconductive NiO surface (red curve).

Finite-element simulations. Finite-element simulations were carried out using COMSOL Multiphysics® version 5.2 commercial simulation package and the results are shown in Figure S8. The full COMSOL modeling report attached to the end of this supplementary materials. Briefly, A 3D model was built to simulate the SECM experiments, including a Pt nanoelectrode and HOPG

substrate with NiO nanosheet. the "transport of dilute species" module was used to solve the diffusion problems involving in the generation/collection experiments. For simulation parameters, the assumed current density at the NiO basal plane is 50 mA/cm^2. This value is comparable to that reported[5] for the NiO nanosheet at +1.57 V vs. RHE and corresponds to the tip current over NiO in a reasonable agreement with the experiment. However, the simulations in Fig. S8 are only semiquantitative. Some experimental issues, such as the non-zero background current due to the oxygen production at a macroscopic NiO substrate and Fc contribution to SG/TC signal have not been included in these simulations.

Cyclic voltammograms of OER at the HOPG and NiO/HOPG. The voltammograms of OER at the NiO/HOPG and bare HOPG substrates and i_T vs. E_S curves (Figure S3) were obtained to optimize the imaging parameters, such as tip and substrate potentials. The substrate potential was linearly swept from 0 to 0.9 V, and the tip potential was held at -0.6 V, so that oxygen generated at the substrate was reduced at the tip. From the substrate voltammograms (Fig. S3A), one can see that the oxidation of water at drop-cast NiO occurs at $E_S > 0.6$ V; while no appreciable OER current flows at bare HOPG up to $E_S = 0.9$ V. The corresponding i_T vs. E_S curves (Fig. S3B) show the reduction of oxygen generated at NiO at $E_S > 0.6$ V and no such current over the bare HOPG substrate at E_S up to 0.9 V.

Evaluation of spatial resolution. Since the first attempt to estimate the SECM resolution from simulations[6], it was often assumed be of the order of the tip radius; but this is a conservative order-of-magnitude estimate. To demonstrate the best resolution that we could achieve with the system, we provide Supplementary Figure S7 showing line scans over the HOPG/NiO boundary (The line scans were obtained with the SECM tip similar to the one used in Fig. 3; $a \approx 20$ nm.) It is worth noting that because the total acquisition time is shorter, less dioxygen molecules were produced

while obtaining the line scans than during the imaging in Fig. 3b. Therefore, the peaks in these line scans are narrower than those in Fig. 3.

Supplementary Figure S9 shows the analysis of the line scans over the HOPG/NiO boundary from Figure S7 that can be used to evaluate the lateral resolution of our reactivity maps. The width of the current profile in Suppl. Fig. S9 is not numerically equal to spatial resolution. To the first order approximation, the measured profile is a convolution between the point spread function of the tip, diffusion broadening, and the underlying reactivity structures—which in our case is not a delta function. Therefore, the measured peak width is always larger than the point spread function of the SECM instrument. The line scans were deconvolved into a linear combination of a Gaussian function and a Z-shaped membership function. The lower bound of our resolution can be calculated by measuring the full width at half maximum of the Gaussian function. The full width averaged over the four scans is 16.5 ± 0.3 nm. This number is close to the 20 nm effective tip radius in Figs. 3 and S7. It should be noted that our instrumental resolution is better than this number because the full width measurement includes the width of the underlying (100) facet. Therefore, the attained spatial resolution is of the order of 15 nm.

Supplementary figures:

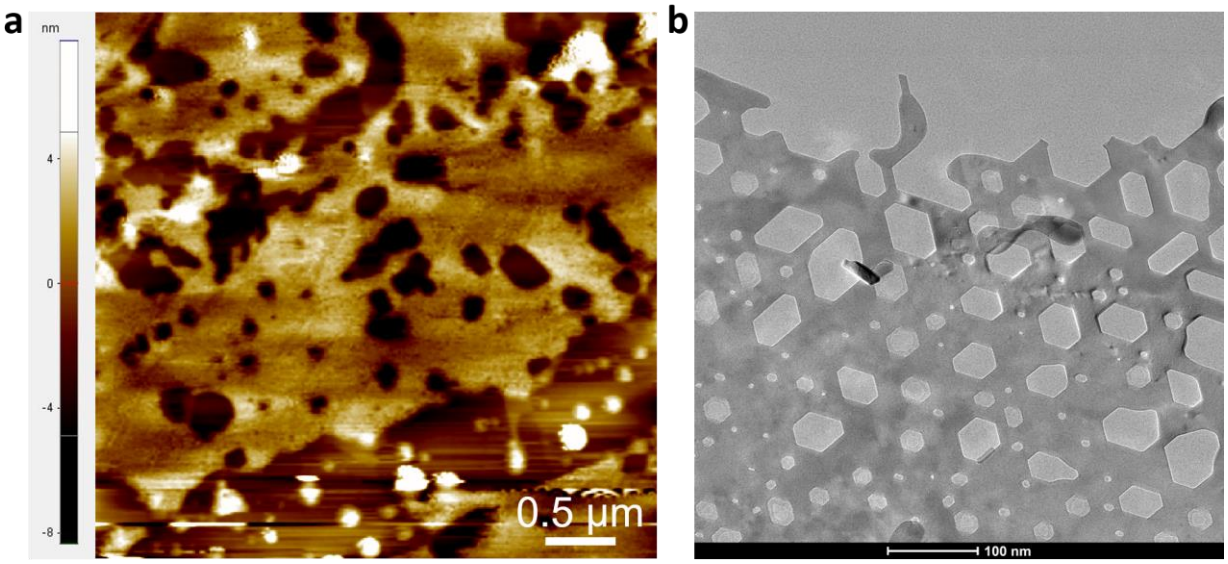

Supplementary Figure S1. (a) AFM image of the 2-D NiO nanosheet with sub-micrometer defects lying flat on the HOPG surface. (b) Bright field transmission electron microscopy (BF-TEM) image of the NiO nanosheet.

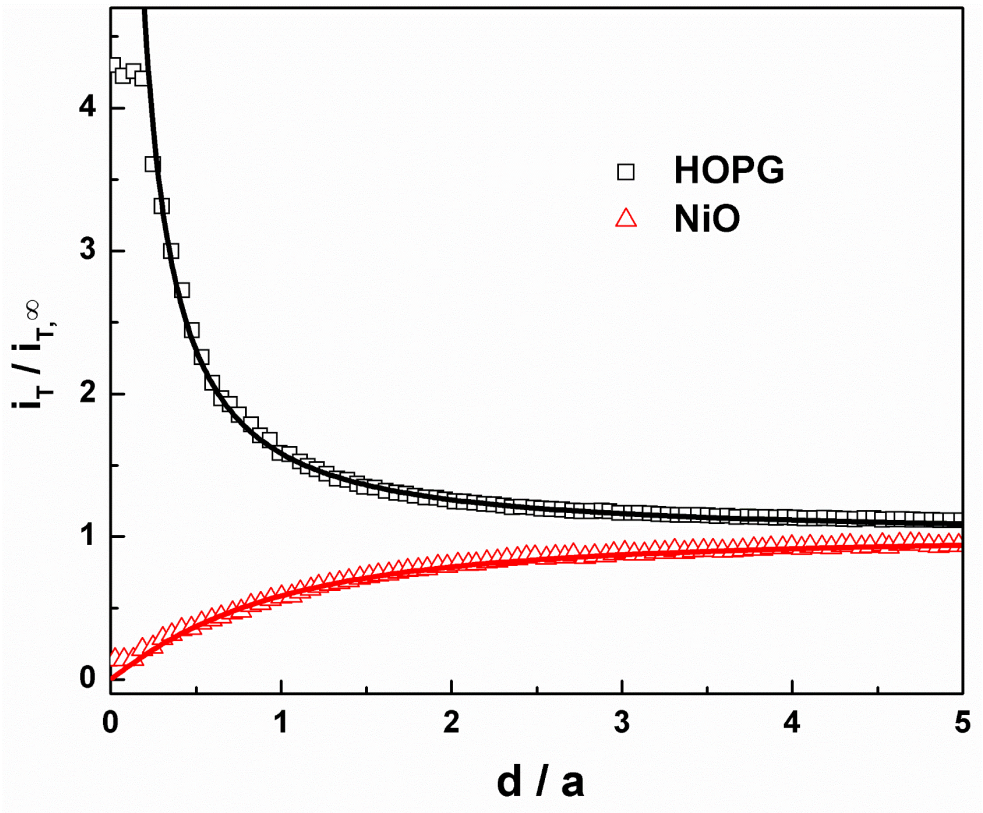

Supplementary Figure S2. The experimental positive and negative feedback responses (symbols) and corresponding theoretical curves (solid lines) of the ferrocenemethanol at conductive HOPG surface and semiconductor NiO surface. Solution contained 1 mM FcMeOH and 0.1 M KCl. The tip potential was 0.5 V vs. Ag/AgCl and the substrate was unbiased. In this figure, *d* denotes the distance between the tip and the substrate surface, *a* denotes the radius of the tip electrode; *a* = 80 nm.

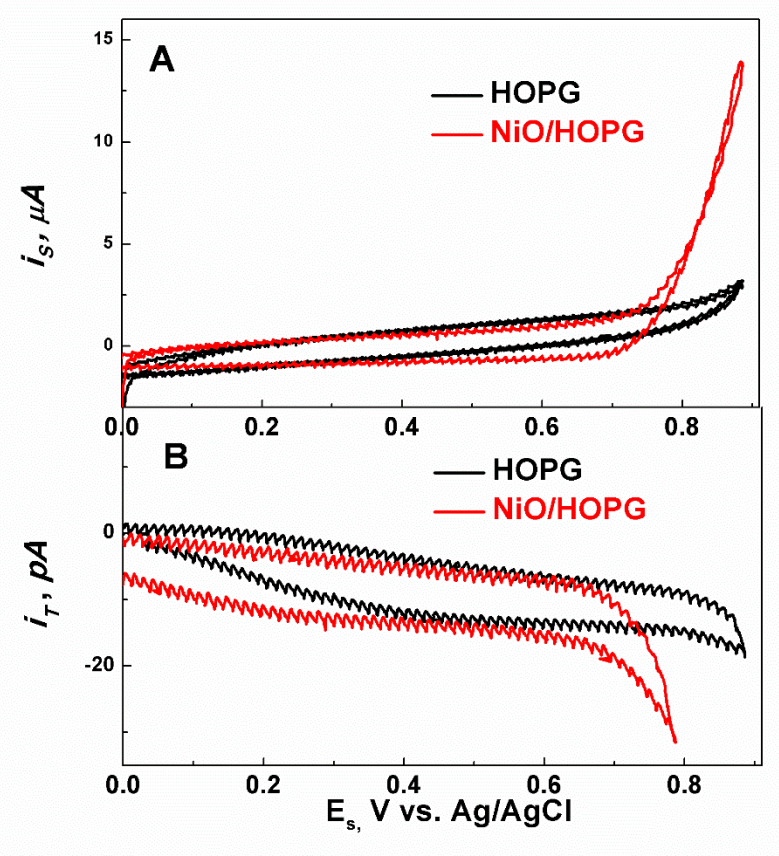

Supplementary Figure S3. (A) substrate voltammograms and (B) i_T vs. E_S curves for the OER at the NiO/HOPG (red curves) and bare HOPG (black curves) substrate and the reduction of the generated O_2 at the 80-nm-radius Pt tip. d = 100 nm. v = 100 mV/s. Solution contained 0.001 M KOH and 0.1 M KCl. E_T = -0.6 V vs Ag/AgCl.

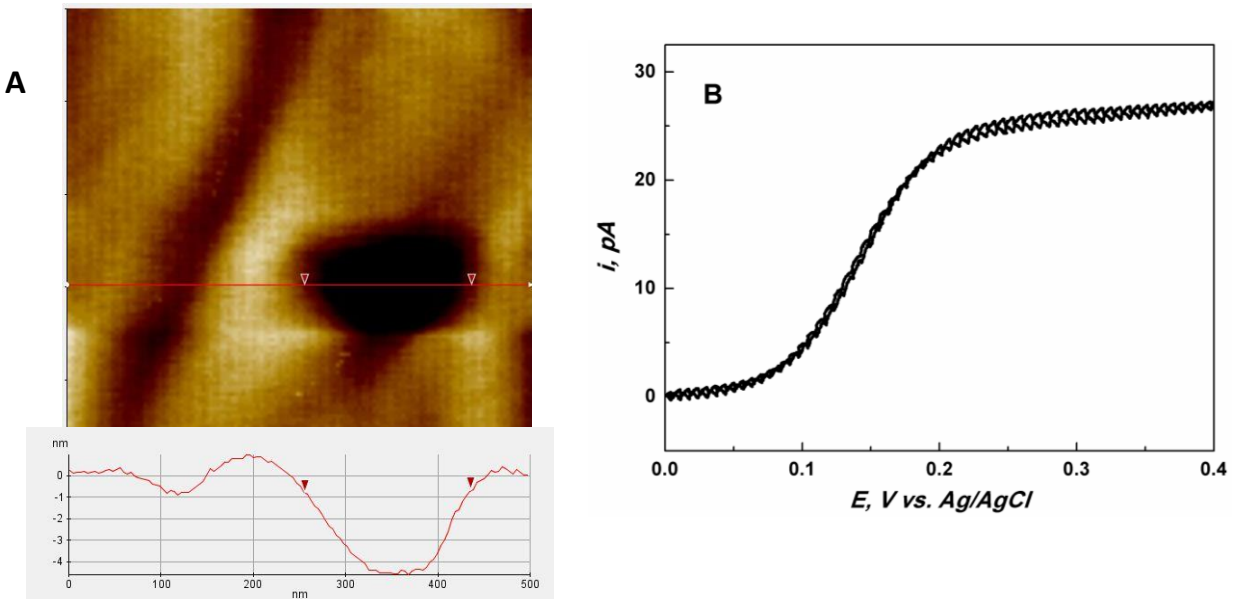

Supplementary Figure S4. (A) Noncontact-mode AFM topographic image of and (B) steady-state voltammogram of 1 mM Fc in 0.1 M KCl solution obtained at the 80 nm-radius polished Pt tip. The red line in (A) corresponds to the shown cross-section.

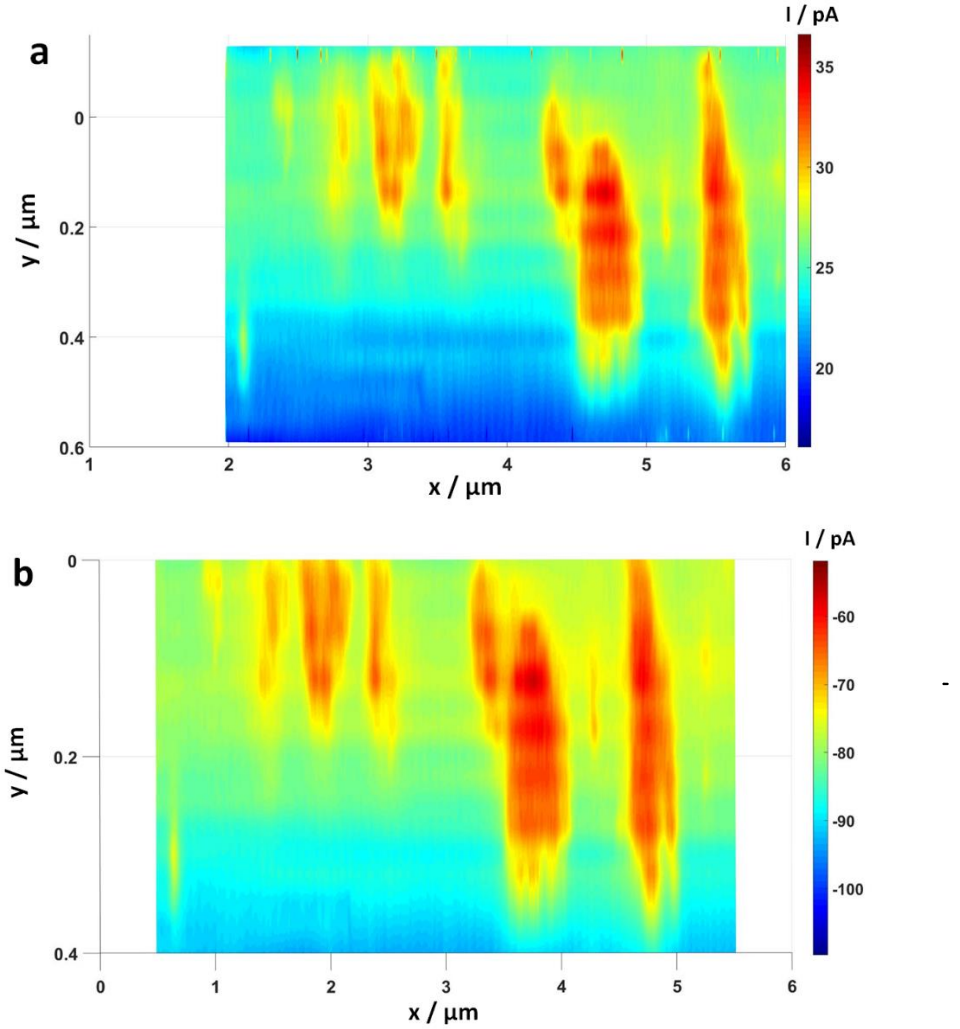

Supplementary Figure S5. 2D SECM color maps of the NiO nanosheet with defect holes corresponding to the 3D images in Figure 2.

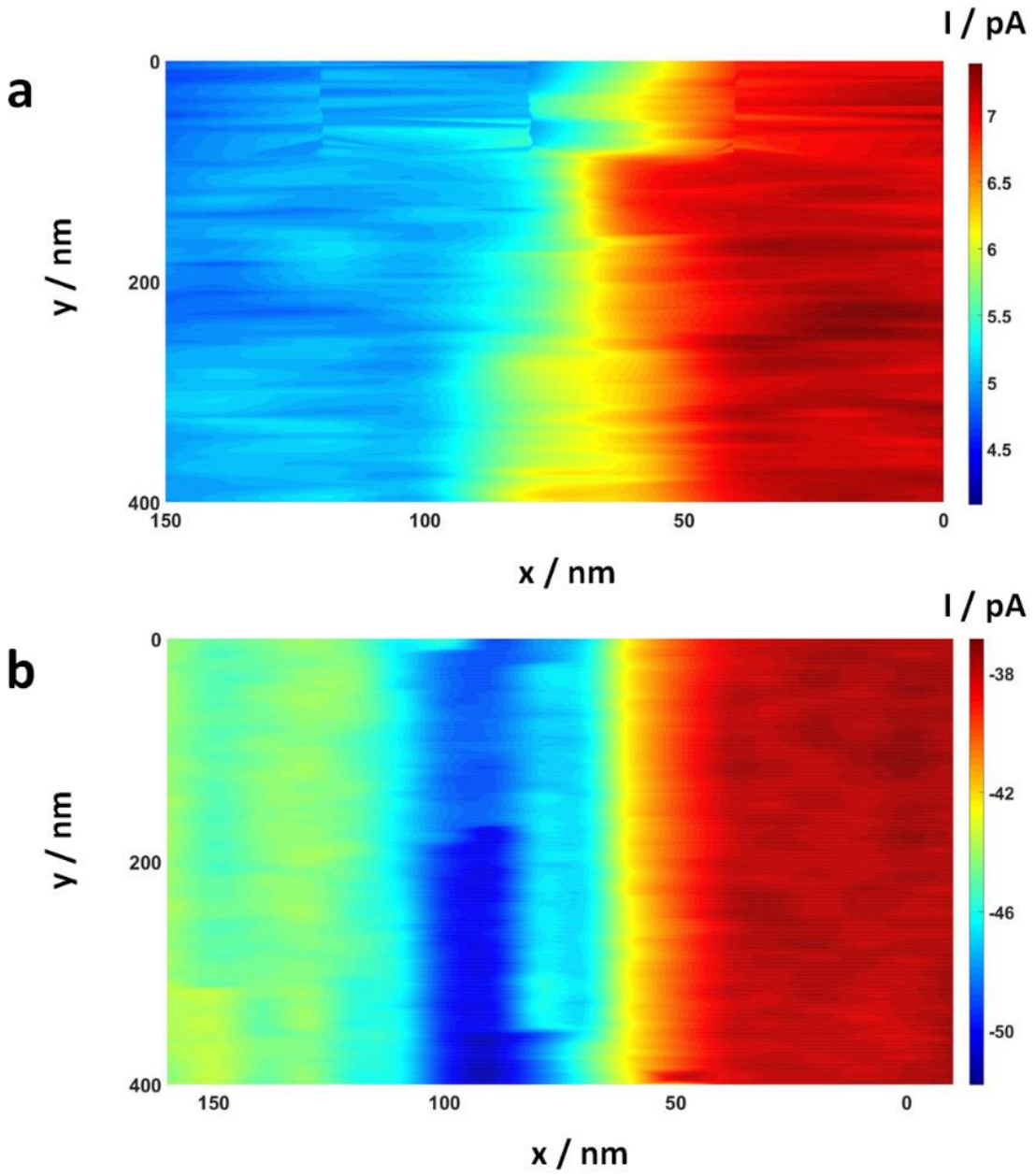

Supplementary Figure S6. 2D SECM color maps of the NiO edge corresponding to the 3D images of Figure 3.

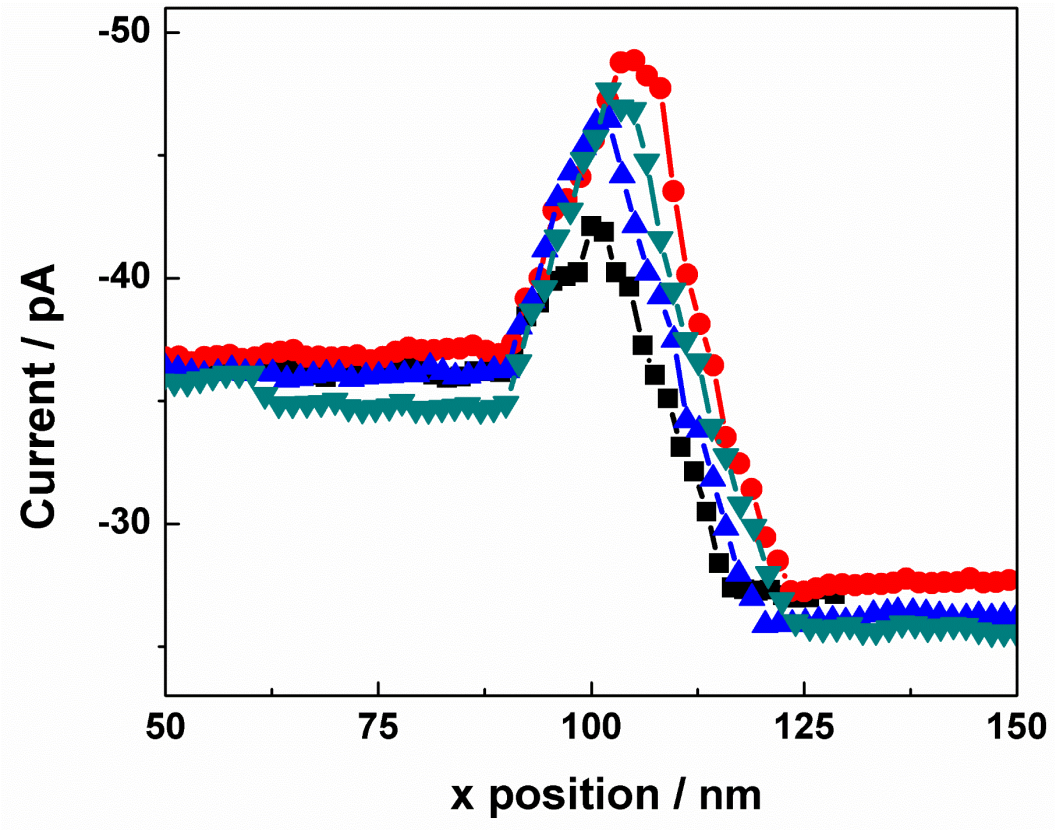

Supplementary Figure S7. Four experimental line scans across the NiO nanosheet edge recorded in the SG/TC mode. Tip radius, $a \approx 20$ nm. For other parameters, see Fig. 3B.

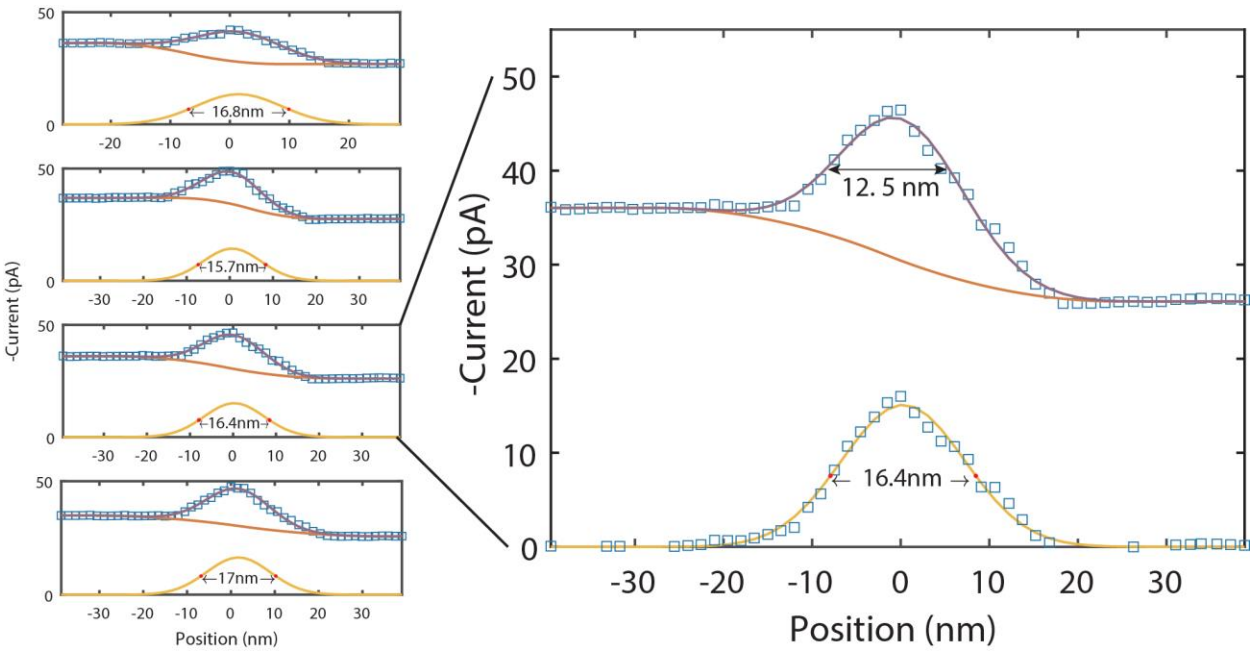

Supplementary Figure S8. Analysis of the lines scans in Supplementary Figure S7. The measured full width at half maximum averaged over the four scans is 16.5 ± 0.3 nm.

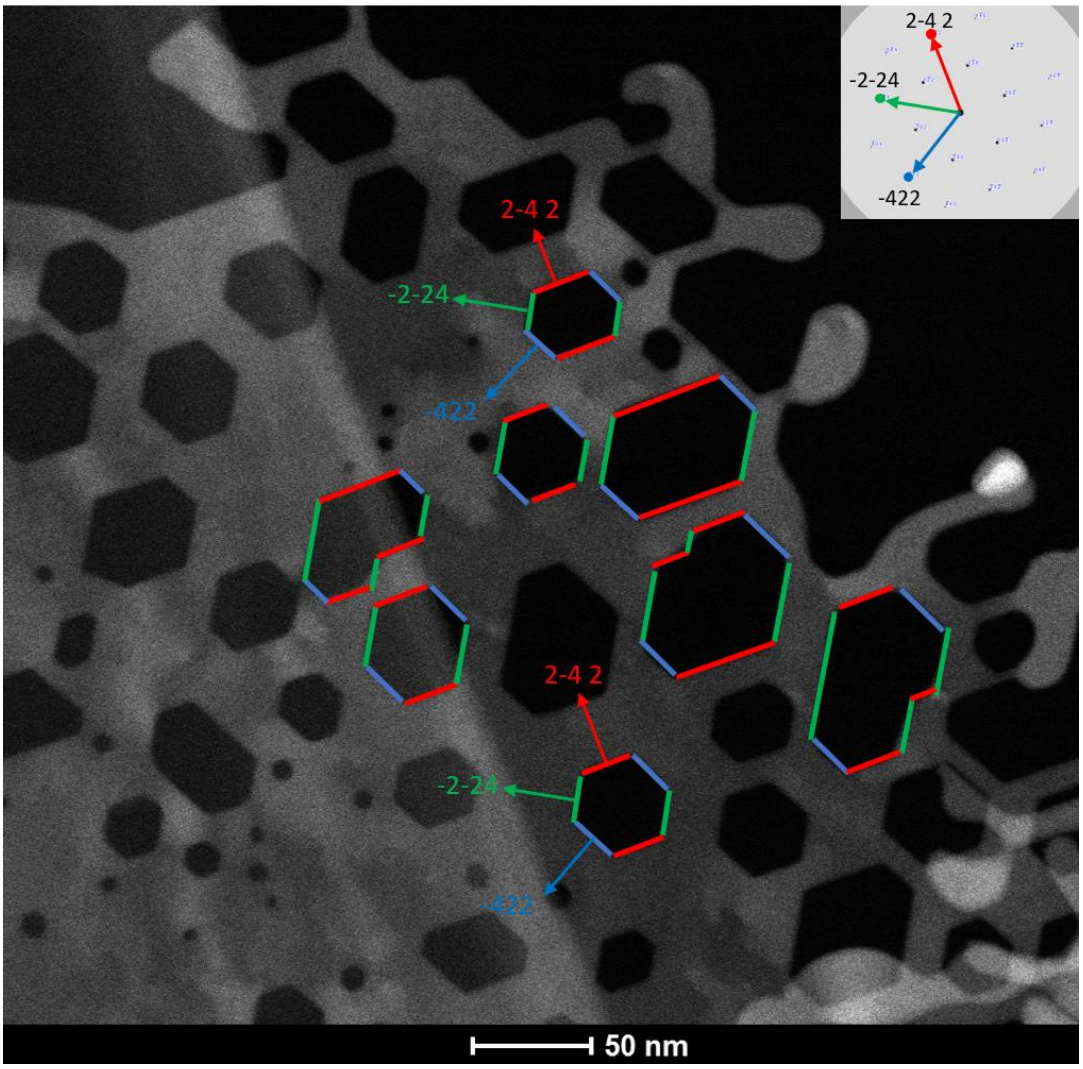

Supplementary Figure S9. Image showing that nearly all large defect holes are terminated with crystallographically identical <112> edges.

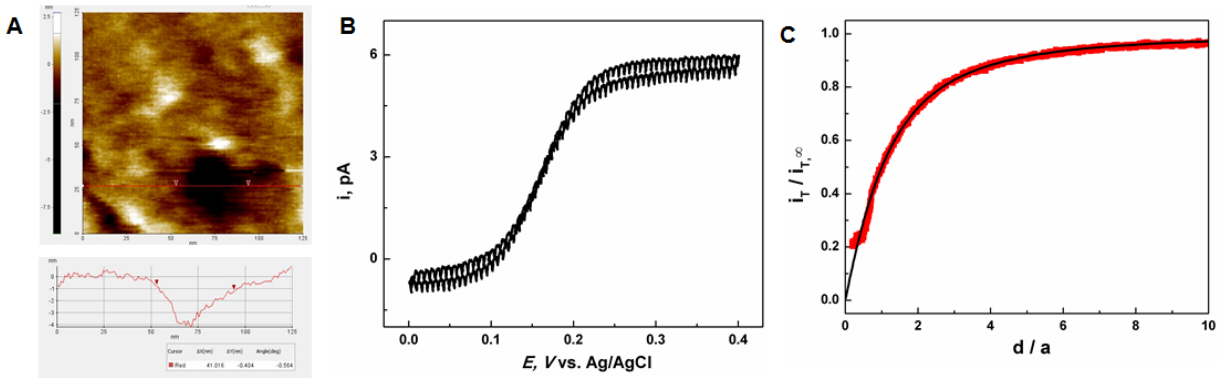

Supplementary Figure S10. (A) Noncontact-mode AFM topographic image of the 20 nm-radius polished Pt tip, and (B) steady-state voltammogram and (C) experimental (red dots) and theoretical (black curve; pure negative feedback) approach curves obtained with the same electrode. Solution contained 1 mM Fc in 0.1 M KCl. The red line in (A) corresponds to the shown cross-section.

References

1. Sun, P.;Mirkin, M. V. Kinetics of electron-transfer reactions at nanoelectrodes. *Analytical Chemistry* **2006**, 78, 6526-6534.
2. Wang, Y. X.; Kececi, K.; Velmurugan, J.;Mirkin, M. V. Electron transfer/ion transfer mode of scanning electrochemical microscopy (SECM): a new tool for imaging and kinetic studies. *Chemical Science* **2013**, 4, 3606-3616.
3. Nogala, W.; Velmurugan, J.;Mirkin, M. V. Atomic Force Microscopy of Electrochemical Nanoelectrodes. *Analytical Chemistry* **2012**, 84, 5192-5197.
4. Midgley, P.;Weyland, M. 3D electron microscopy in the physical sciences: the development of Z-contrast and EFTEM tomography. *Ultramicroscopy* **2003**, 96, 413-431.
5. Xu, Y.; Huang, K.; Ou, G.; Tang, H.; Wei, H.; Zhang, Q.; Gong, J.; Fang, M.;Wu, H. A facile fabrication method for ultrathin NiO/Ni nanosheets as a high-performance electrocatalyst for the oxygen evolution reaction. *RSC Advances* **2017**, 7, 18539-18544.
6. Bard, A. J.; Mirkin, M. V.; Unwin, P. R.;Wipf, D. O. Scanning electrochemical microscopy. 12. Theory and experiment of the feedback mode with finite heterogeneous electron-transfer kinetics and arbitrary substrate size. *The Journal of Physical Chemistry* **1992**, 96, 1861-1868.

COMSOL Report

Contents

1 Global Definitions

Date	Oct 16, 2017 12:02:22 PM

Global settings

Name	Test 3D model 2.mph
Path	C:\Users\Remsen 025\Desktop\New folder (2)\simulation date\NiO edge simulation\test 3D model_2.mph
Version	COMSOL 5.3 (Build: 248)

Used products

COMSOL Multiphysics
Chemical Reaction Engineering Module

1.1 Parameters 1

Parameters

Name	Expression	Value	Description
a	0.02[um]	2E−8 m	
RG	6*a	1.2E−7 m	
d	25e-3	0.025	
x_position	2.5[um]	2.5E−6 m	
y_position	2[um]	2E−6 m	
c1	4	4	
E1	0.5[V]	0.5 V	
k0	10[cm/s]	0.1 m/s	
E0	0[V]	0 V	
k	10	10	
E2	0.7[V]	0.7 V	
Etip	-1[V]	−1 V	

2 Component 1

Settings

Description	Value
Unit system	Same as global system

2.1 Definitions

2.1.1 Coordinate Systems

Boundary System 1

Coordinate system type	Boundary system
Tag	sys1

Settings

First	Second	Third
t1	t2	n

2.2 Geometry 1

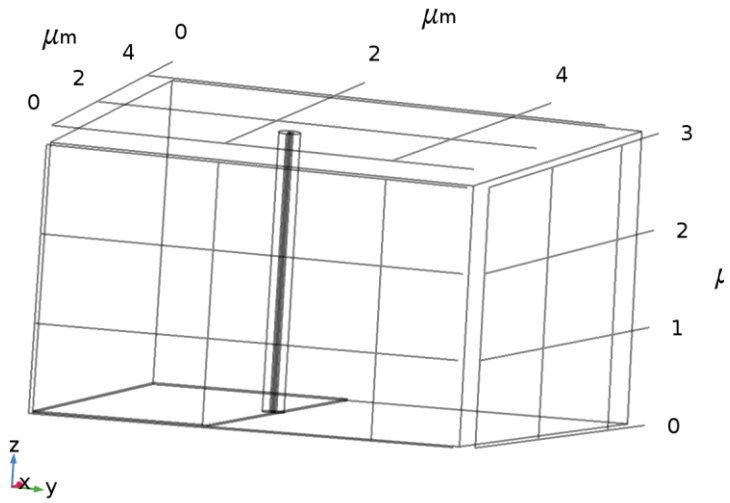

Geometry 1

Units

Length unit	µm
Angular unit	deg

Geometry statistics

Description	Value
Space dimension	3
Number of domains	4
Number of boundaries	24
Number of edges	47
Number of vertices	30

2.2.1 Block 1 (blk1)

Position

Description	Value
Position	{0, 0, 0}

Axis

Description	Value
Axis type	z - axis

Size and shape

Description	Value
Width	5
Depth	5
Height	3

2.2.2 Block 2 (blk2)

Position

Description	Value
Position	{0, 0, 0}

Axis

Description	Value
Axis type	z - axis

Size and shape

Description	Value
Width	5
Depth	2
Height	15e-3

2.2.3 Block 5 (blk5)

Position

Description	Value
Position	{2.5, 2.5, 0}
Base	Center

Axis

Description	Value
Axis type	z - axis

Size and shape

Description	Value
Width	0.4
Depth	0.4
Height	15e-3

2.2.4 Cylinder 1 (cyl1)

Position

Description	Value
Position	{x_position, y_position, d}

Axis

Description	Value
Axis type	z - axis

Size and shape

Description	Value
Radius	a
Height	3 - d

2.2.5 Cylinder 3 (cyl3)

Position

Description	Value
Position	{x_position, y_position, d}

Axis

Description	Value
Axis type	z - axis

Size and shape

Description	Value
Radius	RG
Height	3 - d

2.3 Transport of Diluted Species

Used products

COMSOL Multiphysics
Chemical Reaction Engineering Module

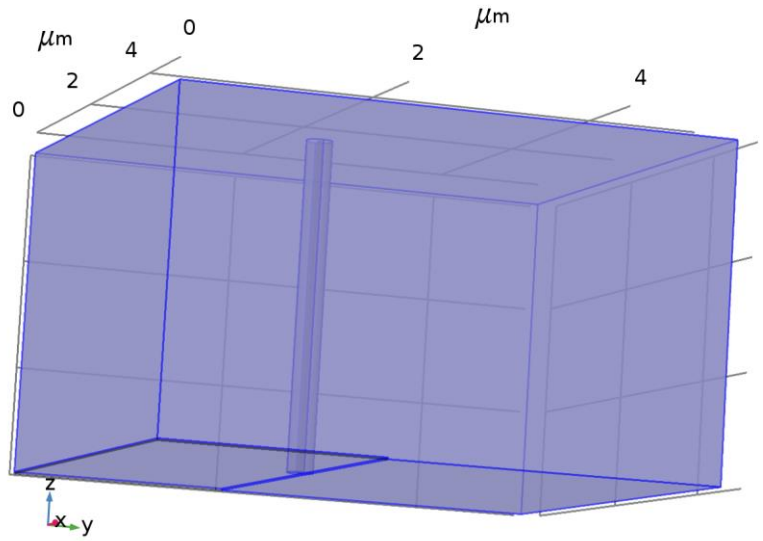

Transport of Diluted Species

Selection

Geometric entity level	Domain
Selection	Domain 2

Equations

$$\nabla \cdot (-D_i \nabla c_i) = R_i$$
$$\mathbf{N}_i = -D_i \nabla c_i$$

2.3.1 Interface settings

Transport mechanisms

Settings

Description	Value
Convection	Off
Migration in electric field	Off
Mass transfer in porous media	Off

2.3.2 Variables

Name	Expression	Unit	Description	Selection	Details
tds.R_cO	0	mol/(m^3·s)	Total rate expression	Domain 2	+ operation
tds.R_cR	0	mol/(m^3·s)	Total rate expression	Domain 2	+ operation
tds.epsilon_p	1	1	Porosity	Domain 2	
tds.theta	tds.epsilon_p	1	Liquid volume fraction	Domain 2	
tds.av	0	1	Gas volume fraction	Domain 2	
tds.nx	unx	1	Normal vector, x component	Boundaries 6, 8, 11–13, 17, 19, 22	
tds.ny	uny	1	Normal vector, y component	Boundaries 6, 8, 11–13, 17, 19, 22	
tds.nz	unz	1	Normal vector, z component	Boundaries 6, 8, 11–13, 17, 19, 22	
tds.nx	dnx	1	Normal vector, x component	Boundaries 4–5, 7, 9–10, 24	
tds.ny	dny	1	Normal vector, y component	Boundaries 4–5, 7, 9–10, 24	
tds.nz	dnz	1	Normal vector, z component	Boundaries 4–5, 7, 9–10, 24	
tds.nxmesh	unxmesh	1	Normal vector (mesh), x component	Boundaries 6, 8, 11–13, 17, 19, 22	

Name	Expression	Unit	Description	Selection	Details
tds.nymesh	unymesh	1	Normal vector (mesh), y component	Boundaries 6, 8, 11–13, 17, 19, 22	
tds.nzmesh	unzmesh	1	Normal vector (mesh), z component	Boundaries 6, 8, 11–13, 17, 19, 22	
tds.nxmesh	dnxmesh	1	Normal vector (mesh), x component	Boundaries 4–5, 7, 9–10, 24	
tds.nymesh	dnymesh	1	Normal vector (mesh), y component	Boundaries 4–5, 7, 9–10, 24	
tds.nzmesh	dnzmesh	1	Normal vector (mesh), z component	Boundaries 4–5, 7, 9–10, 24	
tds.nxc	-root.nxc/tds.ncLen	1	Normal vector, x component	Boundaries 6, 8, 11–13, 17, 19, 22	
tds.nyc	-root.nyc/tds.ncLen	1	Normal vector, y component	Boundaries 6, 8, 11–13, 17, 19, 22	
tds.nzc	-root.nzc/tds.ncLen	1	Normal vector, z component	Boundaries 6, 8, 11–13, 17, 19, 22	
tds.nxc	root.nxc/tds.ncLen	1	Normal vector, x component	Boundaries 4–5, 7, 9–10, 24	
tds.nyc	root.nyc/tds.ncLen	1	Normal vector, y component	Boundaries 4–5, 7, 9–10, 24	
tds.nzc	root.nzc/tds.ncLen	1	Normal vector, z component	Boundaries 4–5, 7, 9–10, 24	
tds.ncLen	sqrt(root.nxc^2+root.nyc^2+root.nzc^2+eps)	1	Help variable	Boundaries 4–13, 17, 19, 22, 24	

2.3.3 Transport Properties 1

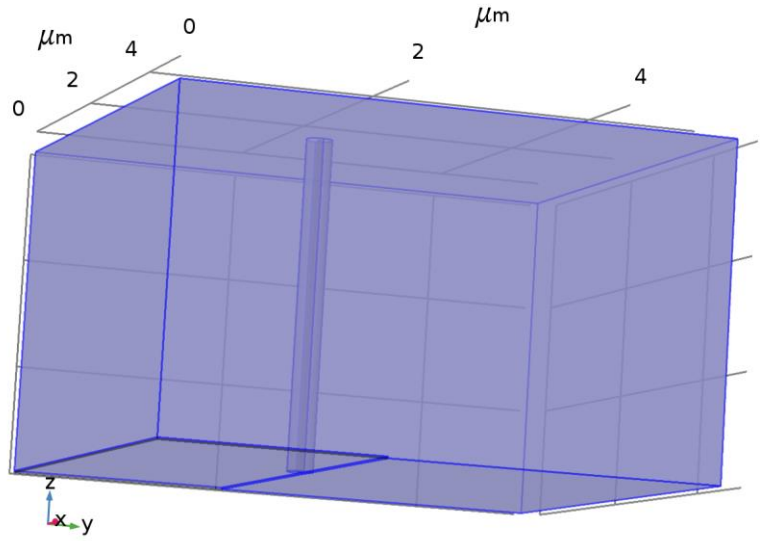

Transport Properties 1

Selection

Geometric entity level	Domain
Selection	Domain 2

Equations

$$\nabla \cdot (-D_i \nabla c_i) = R_i$$
$$\mathbf{N}_i = -D_i \nabla c_i$$

Diffusion

Settings

Description	Value
Material	None
Diffusion coefficient	User defined
Diffusion coefficient	{{2e-9[m^2/s], 0, 0}, {0, 2e-9[m^2/s], 0}, {0, 0, 2e-9[m^2/s]}}
Diffusion coefficient	User defined
Diffusion coefficient	{{5e-9[m^2/s], 0, 0}, {0, 5e-9[m^2/s], 0}, {0, 0, 5e-9[m^2/s]}}
Coordinate system	Global coordinate system
Temperature	User defined
Temperature	293.15[K]

Used products

COMSOL Multiphysics

Shape functions

Name	Shape function	Unit	Description	Shape frame	Selection
cO	Lagrange (Linear)	mol/m^3	Concentration	Spatial	Domain 2
cR	Lagrange (Linear)	mol/m^3	Concentration	Spatial	Domain 2

Weak expressions

Weak expression	Integration order	Integration frame	Selection
-cOt*test(cO)+tds.dflux_cOx*test(cOx)+tds.dflux_cOy*test(cOy)+tds.dflux_cOz*test(cOz)	2	Spatial	Domain 2
-cRt*test(cR)+tds.dflux_cRx*test(cRx)+tds.dflux_cRy*test(cRy)+tds.dflux_cRz*test(cRz)	2	Spatial	Domain 2
tds.streamline*(isScalingSystemDomain==0)	2	Spatial	Domain 2
tds.crosswind*(isScalingSystemDomain==0)	4	Spatial	Domain 2

2.3.4 No Flux 1

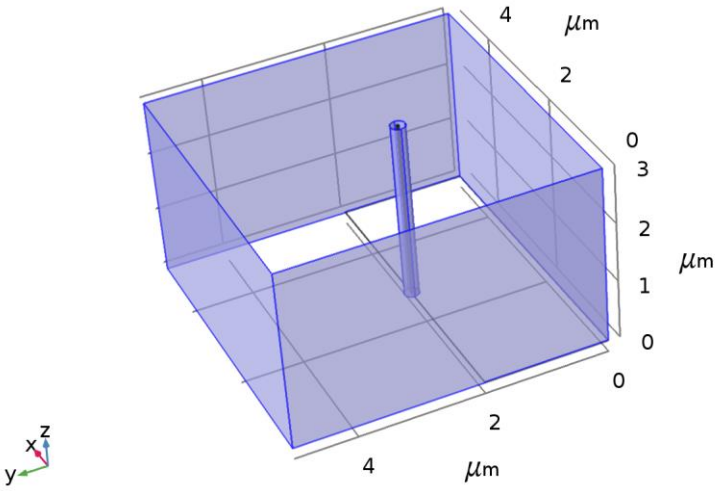

No Flux 1

Selection

Geometric entity level	Boundary

Selection	Boundaries 4–5, 10–13, 19, 22, 24

Equations

$$-\mathbf{n} \cdot \mathbf{N}_i = 0$$

Used products

COMSOL Multiphysics

2.3.5 Initial Values 1

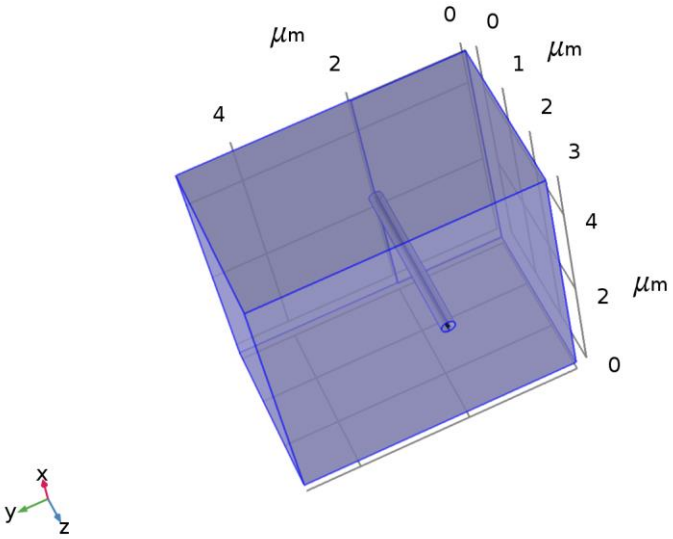

Initial Values 1

Selection

Geometric entity level	Domain
Selection	Domain 2

Initial values

Settings

Description	Value
Concentration	{0, 10}

Used products

COMSOL Multiphysics

2.3.6 Concentration 2

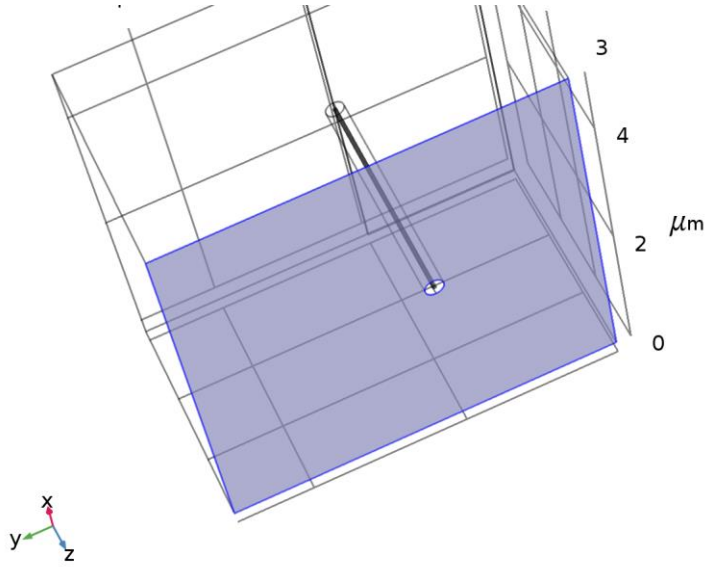

Concentration 2

Selection

Geometric entity level	Boundary
Selection	Boundary 7

Equations

$$c_i = c_{0,i}$$

Concentration

Settings

Description	Value
Species cO	On
Species cR	On
Concentration	{0, 10}

Used products

COMSOL Multiphysics

Variables

Name	Expression	Unit	Description	Selection
tds.c0_cO	0	mol/m^3	Concentration	Boundary 7
tds.c0_cR	10	mol/m^3	Concentration	Boundary 7

Constraints

Constraint	Constraint force	Shape function	Selection	Details
-cO+tds.c0_cO	test(-cO+tds.c0_cO)	Lagrange (Linear)	Boundary 7	Elemental
-cR+tds.c0_cR	test(-cR+tds.c0_cR)	Lagrange (Linear)	Boundary 7	Elemental

2.3.7 Flux 1

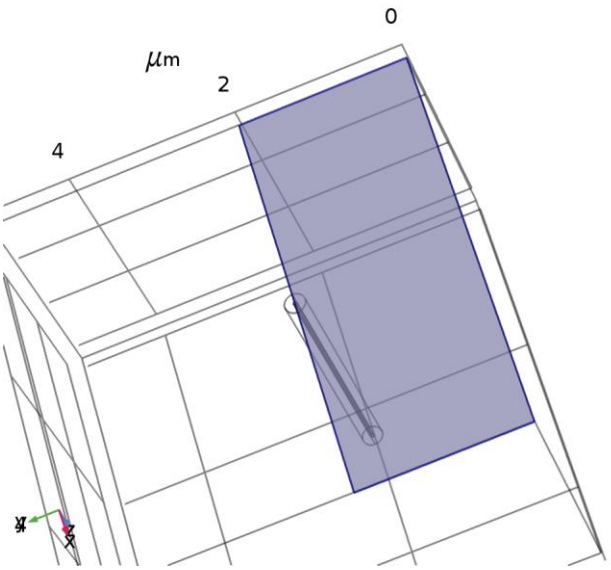

Flux 1

Selection

Geometric entity level	Boundary
Selection	Boundary 6

Equations

$$-\mathbf{n} \cdot \mathbf{N}_i = N_{0,i}$$

Inward flux

Settings

Description	Value
Flux type	General inward flux
Species cO	On
Species cR	On
	{0.005, -0.005}

Used products

COMSOL Multiphysics

Weak expressions

Weak expression	Integration order	Integration frame	Selection
0.005*test(cO)	2	Spatial	Boundary 6
-0.005*test(cR)	2	Spatial	Boundary 6

2.3.8 Flux 2

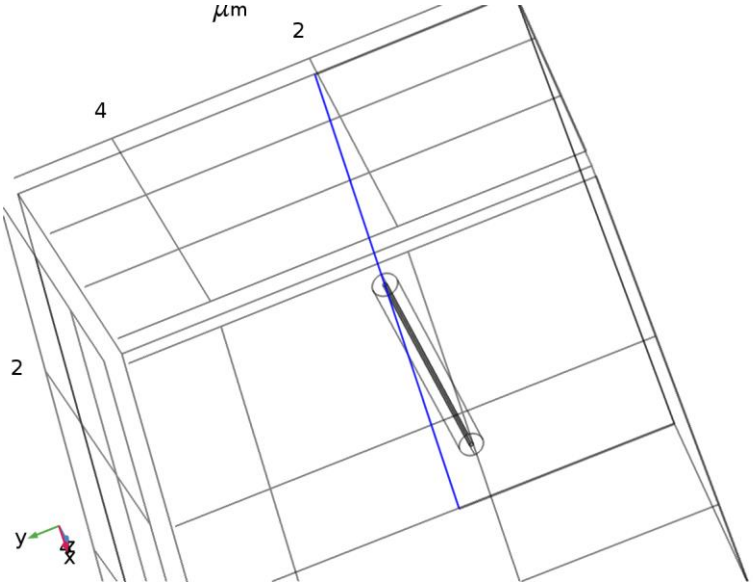

Flux 2

Selection

Geometric entity level	Boundary
Selection	Boundary 8

Equations

$$-\mathbf{n} \cdot \mathbf{N}_i = N_{0,i}$$

Inward flux

Settings

Description	Value
Flux type	General inward flux
Species cO	On
Species cR	On
	{k, -k}

Used products

COMSOL Multiphysics

Weak expressions

Weak expression	Integration order	Integration frame	Selection
k*test(cO)	2	Spatial	Boundary 8
-k*test(cR)	2	Spatial	Boundary 8

2.3.9 Concentration 4

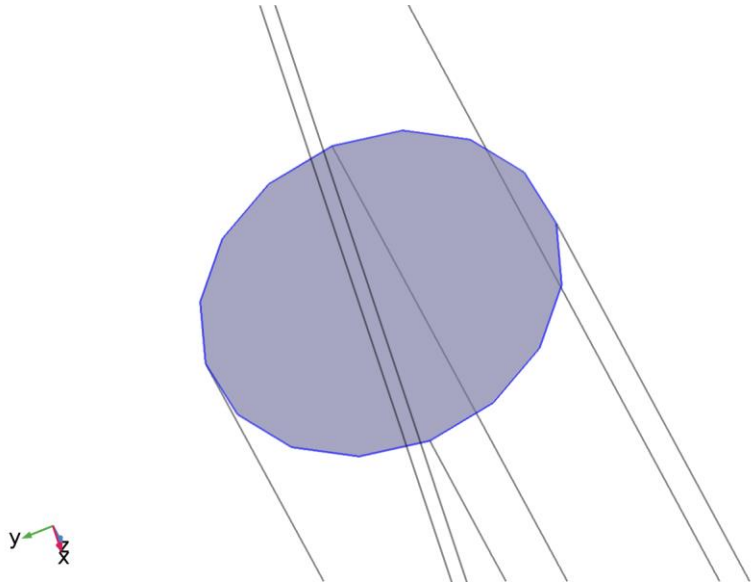

Concentration 4

Selection

Geometric entity level	Boundary
Selection	Boundary 17

Equations

$$c_i = c_{0,i}$$

Concentration

Settings

Description	Value
Species cO	On
Species cR	Off
Concentration	{0, 0}

Used products

COMSOL Multiphysics

Variables

Name	Expression	Unit	Description	Selection
tds.c0_cO	0	mol/m^3	Concentration	Boundary 17

Constraints

Constraint	Constraint force	Shape function	Selection	Details
-cO+tds.c0_cO	test(-cO+tds.c0_cO)	Lagrange (Linear)	Boundary 17	Elemental
0	0	Lagrange (Linear)	Boundary 17	Elemental

2.3.10 Concentration 5

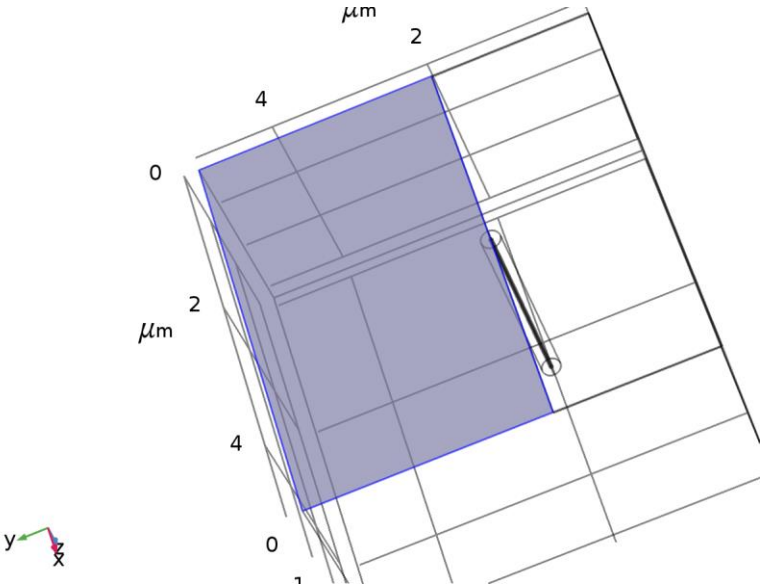

Concentration 5

Selection

Geometric entity level	Boundary
Selection	Boundary 9

Equations

$$c_i = c_{0,i}$$

Concentration

Settings

Description	Value
Species cO	On
Species cR	On
Concentration	{0, 10}

Used products

COMSOL Multiphysics

Variables

Name	Expression	Unit	Description	Selection
tds.c0_cO	0	mol/m^3	Concentration	Boundary 9
tds.c0_cR	10	mol/m^3	Concentration	Boundary 9

Constraints

Constraint	Constraint force	Shape function	Selection	Details
-cO+tds.c0_cO	test(-cO+tds.c0_cO)	Lagrange (Linear)	Boundary 9	Elemental
-cR+tds.c0_cR	test(-cR+tds.c0_cR)	Lagrange (Linear)	Boundary 9	Elemental

2.4 Meshes

2.4.1 Mesh 1

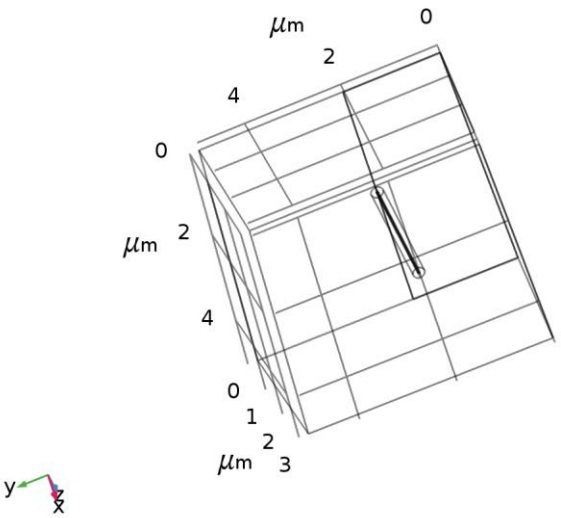

Mesh 1

Size (size)

Settings

Description	Value
Maximum element size	0.175
Minimum element size	0.0075
Curvature factor	0.3
Resolution of narrow regions	0.85

Description	Value
Maximum element growth rate	1.35
Predefined size	Extra fine

Size 1 (size1)

Selection

Geometric entity level	Boundary
Selection	Boundary 6

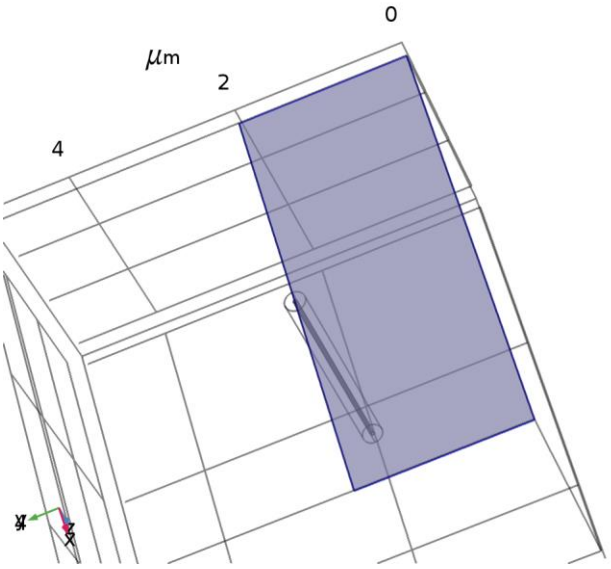

Size 1

Settings

Description	Value
Maximum element size	0.05
Minimum element size	0.002
Minimum element size	Off
Curvature factor	0.2
Curvature factor	Off
Resolution of narrow regions	Off
Maximum element growth rate	1.3
Maximum element growth rate	Off
Predefined size	Extremely fine
Custom element size	Custom

Size 2 (size2)

Selection

Geometric entity level	Boundary
Selection	Boundary 8

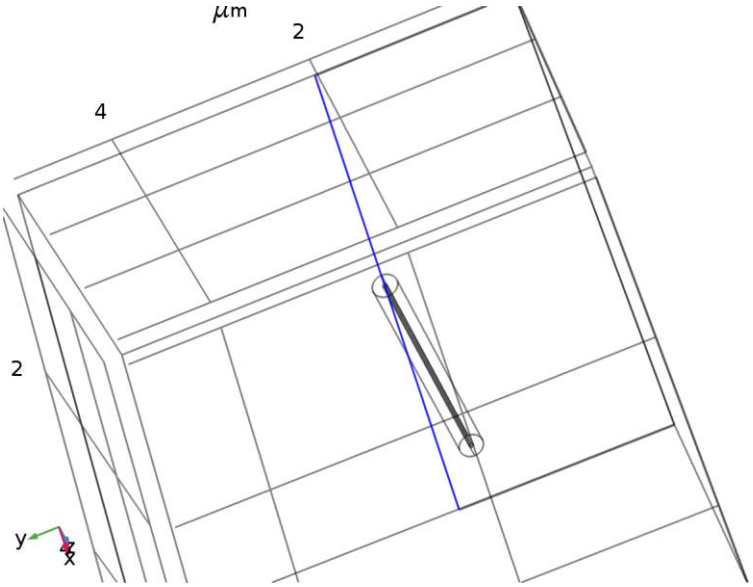

Size 2

Settings

Description	Value
Maximum element size	0.002
Minimum element size	0.015
Minimum element size	Off
Curvature factor	0.3
Curvature factor	Off
Resolution of narrow regions	0.85
Resolution of narrow regions	Off
Maximum element growth rate	1.35
Maximum element growth rate	Off
Predefined size	Extra fine
Custom element size	Custom

Size 3 (size3)

Selection

Geometric entity level	Boundary

Selection	Boundary 17

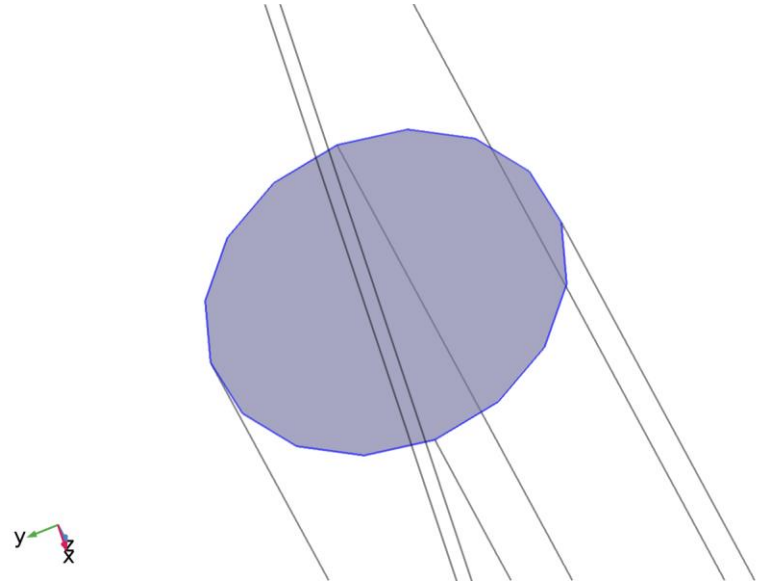

Size 3

Settings

Description	Value
Maximum element size	0.001
Minimum element size	0.09
Minimum element size	Off
Curvature factor	0.6
Curvature factor	Off
Resolution of narrow regions	0.5
Resolution of narrow regions	Off
Maximum element growth rate	1.5
Maximum element growth rate	Off
Custom element size	Custom

Free Tetrahedral 1 (ftet1)

Selection

Geometric entity level	Domain
Selection	Remaining

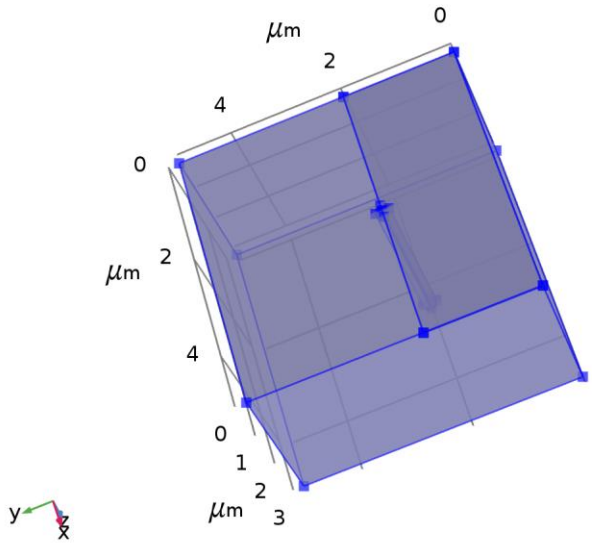

Free Tetrahedral 1

2.4.2 Mesh 2

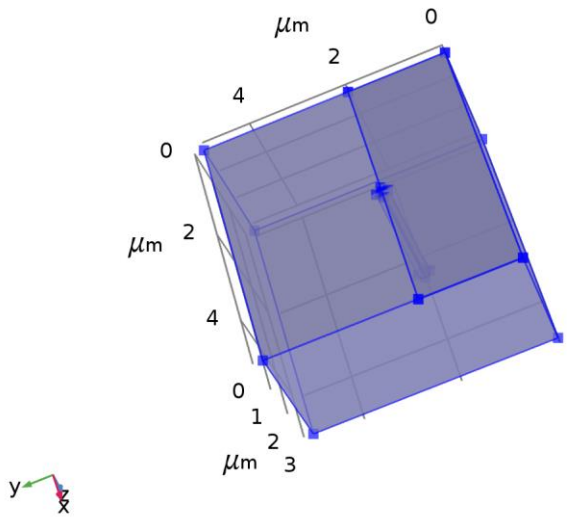

Mesh 2

Size (size)

Settings

Description	Value
Maximum element size	0.5
Minimum element size	0.09
Curvature factor	0.6
Resolution of narrow regions	0.5

Description	Value
Maximum element growth rate	1.5

2.4.3 Mesh 3

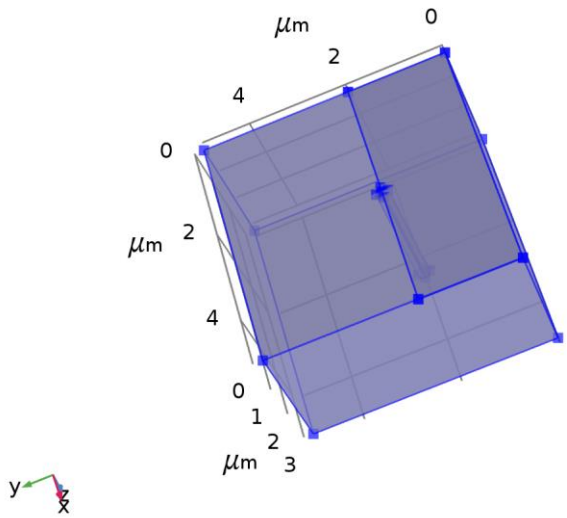

Mesh 3

Size (size)

Settings

Description	Value
Maximum element size	0.5
Minimum element size	0.09
Curvature factor	0.6
Resolution of narrow regions	0.5
Maximum element growth rate	1.5

3 Study 1

Computation information

Computation time	1 h 40 min 1 s
CPU	Intel64 Family 6 Model 94 Stepping 3, 4 cores
Operating system	Windows 10

3.1 Parametric Sweep

Parameter name	Parameter value list	Parameter unit
k	0.005,0.05,0.5,1	
y_position	range(1.9,0.20000000000000018/19,2.1)	um

Study settings

Description	Value
Sweep type	All combinations
Parameter name	{k, y_position}
Unit	{, um}

Parameters

Parameter name	Parameter value list	Parameter unit
k	0.005,0.05,0.5,1	
y_position	range(1.9,0.20000000000000018/19,2.1)	um

3.2 Stationary

Physics and variables selection

Physics interface	Discretization
Transport of Diluted Species (tds)	physics

Mesh selection

Geometry	Mesh
Geometry 1 (geom1)	mesh1

4 Results

4.1 Derived Values

4.1.1 Surface Integration 1

Output

Evaluated in	Table 132

Data

Description	Value
Data set	Study 1/Parametric Solutions 1

Common

Expression	Unit	Description
tds.ntflux_cO*96500[C/mol]	A	

Settings

Description	Value
Integration order	4